Nonlinear Equilibration of Localized Instabilities on a Baroclinic Jet

TIMOTHY M. DELSOLE

Division of Applied Sciences, Harvard University, Cambridge, Massachusetts

BRIAN F. FARRELL

Department of Earth and Planetary Sciences, Harvard University, Cambridge, Massachusetts

(Manuscript received 10 September 1993, in final form 19 January 1994)

ABSTRACT

Dynamical mechanisms underlying the equilibration of absolute instability are examined in a nonlinear, quasigeostrophic, two-layer model. The key to understanding the nonlinear equilibration is in recognizing that linear absolute instabilities can be stabilized both by a reduction of the vertical shear and by enhancement of the mean barotropic velocity. In a localized domain, the equilibration process proceeds with the creation of locally convectively unstable regions downstream, which encroach onto the locally absolutely unstable region until the local instability is suppressed. That local instabilities exist only if absolutely unstable regions span a minimum size is verified by eigenvalue calculations of three-dimensional flows. Numerical examples suggest that this critical size is at least 9000 km for a wide range of parameter values chosen to investigate the midlatitude storm tracks. Fluctuations arising from local absolute instability obtain maximum amplitude in the downstream convectively unstable regions rather than in the absolutely unstable regions themselves. Together, these results suggest that if an equilibrated absolute instability were to occur in midlatitudes, a zonal band of surface easterlies exceeding 9000 km would be required and the associated enhanced variances would not be found coincident with the regions of absolute instability.

1. Introduction

Geopotential height fluctuations with 2–6-day period are concentrated in the oceanic storm tracks off the east coasts of North America and Asia (Blackmon et al. 1977). Theoretical work seeking an explanation for this localization of variance has recently been stimulated by the development of the concept of absolute instability (Merkine 1977; Farrell 1982, 1983; Lindzen et al. 1983; Pierrehumbert 1984; Cai and Mak 1990). Absolute instability can be understood by considering the linear asymptotic response to a localized impulse in an unstable system: the dominant asymptotic response arises from a superposition of unstable normal modes forming an envelope that both propagates and expands as it grows. If the growing envelope remains in the region of the original impulse, the system is said to be absolutely unstable. If the growing envelope propagates away from the region of the original impulse, the system is said to be convectively unstable.

Application of the concepts of absolute and convective instability to zonally varying flows and to periodic systems is not always straightforward. Pierrehumbert (1984) succeeded in applying WKB analysis to a basic state that varied in both the zonal and vertical direction and introduced the formal distinctions between local and global instability. A local instability has amplitude maximized in a bounded region and vanishing at infinity. This contrasts with a global instability, which demands periodic boundary conditions for its existence. Pierrehumbert showed, under WKB assumptions, that a necessary condition for local instability is the existence of a region of absolute instability. Thus, the concepts of absolute and convective instability facilitate understanding of local and global instabilities in flows possessing zonal variations in background baroclinicity, barotropic rate of strain, and effective dissipation. In particular, a pulse excited in a region of local convective instability may propagate out of that region and subsequently enter regions less hospitable to growth. A pulse excited in a region of local absolute instability, on the other hand, can remain in the same baroclinic region as it grows. WKB shows that a local instability can exist in the latter case if the unstable region is slowly varying compared to the local wavelength of the instability. Distinguishing between local and global instability is difficult in more complex flows. For instance, if damping in a localized region is sufficiently strong, global modes may be stabilized while local modes may not be; if the damping is less strong, a

Corresponding author address: Timothy DelSole, Code 910.3, NASA Goddard Space Flight Center, Greenbelt, MD 20771.
E-mail: delsole@hera.gsfc.nasa.gov

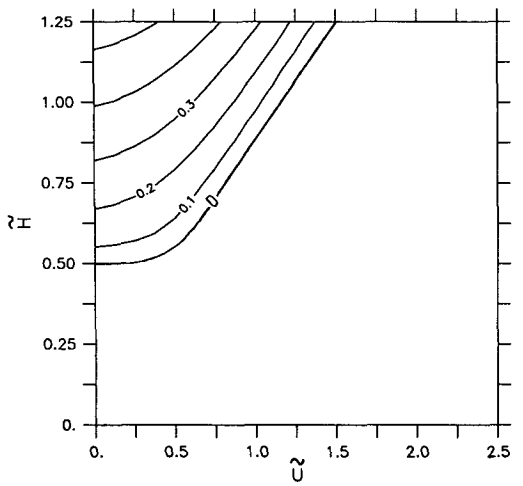

FIG. 1. Contours of absolute instability growth rate for the two-layer model as a function of the nondimensional barotropic velocity ($\tilde{U} = (U_1 + U_2)/2\beta L_R^2$) and baroclinic velocity ($\tilde{H} = (U_1 - U_2)/2\beta L_R^2$). The meridional wavenumber is $l = 0.5$ and the critical baroclinic velocity for instability is $\tilde{H} = 0.5$.

global mode may "tunnel" through to establish its global structure and grow.

Experience has shown that models of baroclinic instability support absolute instability only in the presence of surface easterlies in flows possessing positive shears (Farrell 1982, 1983; Pierrehumbert 1986; Lin and Pierrehumbert 1993). Pedlosky (1989) has suggested that for certain kinds of dispersive waves in two-layer models, the zonal region of absolute instability necessary for local instability can be much smaller than a Rossby radius. Whether this conclusion holds in the full two-layer model and whether this minimum size might differ in a nonlinearly equilibrated flow has yet to be determined. Moreover, it has not yet been determined whether the linear criterion for absolute instability holds in the nonlinear regime. In fact, since the two-layer model is known to exhibit temporal instability persistence at subcritical shear in the nonlinear regime (Lee and Held 1991), the question of whether a similar hysteresis applies to the transition from absolute to convective instability remains open. Finally, the equilibration of absolute instabilities bounded by regions of strong dissipation in the presence of horizontal shear has not been completely understood and its study may provide insight into the physics of nonlinear equilibration of baroclinic waves.

In this work we examine these questions regarding the dynamics of localized disturbances in a nonlinear quasigeostrophic two-layer model. To facilitate the analysis, we filter out global modes by introducing a sponge layer: a localized region of linear relaxation of potential vorticity toward a prescribed flow with a timescale sufficiently short to dissipate any eddy that propagates into it. The sponge is introduced to inhibit recirculation of waves and is not intended to represent a specific damping region in the atmosphere. We have verified that our results are independent of the magnitude of the damping within the sponge, as would be required for local disturbances. In section 2 we discuss a possible nonlinear equilibration mechanism based on simple properties of absolute instability and wave–mean flow interactions. In subsequent sections these ideas are extended by simulating absolute instability in a nonlinear two-layer model.

2. Equilibration of absolute instabilities

As discussed by Briggs (1964) and Merkine (1977), the existence of absolute instability can be determined by examining the dispersion relation in the complex frequency plane. It is a routine procedure to obtain the following dispersion relation for the two-layer quasi-geostrophic model (Pedlosky 1987):

$$\omega = kU + \frac{-k\beta \pm \sqrt{k^2\beta^2\lambda^4 + k^2H^2K^4(K^4 - 2\lambda^4)}}{K^2(K^2 + 2\lambda^2)} \tag{1}$$

for a wave disturbance of the form

$$(\psi_1, \psi_2) \approx e^{ikx+ily-i\omega t}, \tag{2}$$

where $U = (U_1 + U_2)/2$, $H = (U_1 - U_2)/2$, β is the meridional gradient of the Coriolis parameter, $1/\lambda = L_R$ is the Rossby radius of deformation, $K^2 = k^2 + l^2$, U_1, and U_2 are the zonal mean velocities in the upper and lower layer, respectively, and ψ_n is the streamfunction of the nth layer. Absolute instabilities are found by evaluating the solution of the two-layer equations for asymptotically long times while holding the spatial coordinate constant. Standard techniques reveal that the absolute instabilities are associated with saddle points of the dispersion relation (that is, points in which $\partial\omega/\partial k = 0$) and approach the asymptotic form (Briggs 1964)

$$\lim_{t\to\infty}\lim_{x/t\to 0}(\psi_1, \psi_2) \approx \frac{e^{ik_s x - i\omega(k_s)t}}{\sqrt{t}}, \tag{3}$$

where $\omega(k_s)$ and k_s are the complex frequency and wavenumber at the saddle point, respectively. A further analysis is required to ensure the saddle point is properly formed by the coalescence of two k roots (called the "pinch singularity"), but the details will not be repeated here since they can be found in Briggs (1964). The imaginary part of $\omega(k_s)$, which we call the absolute instability growth rate, is shown in Fig. 1 as a function of the following nondimensional velocities:

$$\tilde{U} = (U_1 + U_2)/2\beta L_R^2, \quad \tilde{H} = (U_1 - U_2)/2\beta L_R^2. \tag{4}$$

The neutral curve is well fit by

$$\tilde{U} = 1.4\tilde{H} - 0.2, \quad \tilde{H} > 0.5. \tag{5}$$

The absolute instability growth rate depends on $\tilde{U}$, in contrast to normal-mode growth rates, because the amplitude growth at a point is influenced by both the temporal growth and the spatial propagation. For highly supercritical shears we can neglect the $\tilde{U}$ intercept and take our criterion for instability to be simply

$$\frac{\tilde{U}}{\tilde{H}} < 1.4. \tag{6}$$

Hereafter, we nondimensionalize lengths by Rossby radius and velocities by the shear $\tilde{H}$. In these units, criterion (6) becomes $U < 1.4$ where U is the nondimensional barotropic velocity.

It is worth mentioning at this point that (6) allows absolute instability for positive bottom-layer velocities but not necessarily for positive surface velocities, which are extrapolations of the layer velocities. For instance, under the common extrapolation formula

$$U_{\text{SURFACE}} = \frac{3U_2 - U_1}{2}, \tag{7}$$

the criterion for two-layer absolute instability implied by (5) for the two-layer model is equivalent to

$$U_{\text{SURFACE}} < -0.3(U_1 - U_2) - 0.2\beta L_R^2, \tag{8}$$

which is always negative for positive shears.

Growing baroclinic instabilities transport heat downgradient. Thermal wind balance demands that the resulting reduction of the temperature gradient be accompanied by a reduction of the vertical shear and by a reduction of the available energy of the background state. If only the shear were adjusted, the eddies could equilibrate by reducing this shear to the critical value for instability. It is commonly observed, however, that baroclinic disturbances growing in the presence of barotropic jets with horizontal scales larger than the Rossby radius tend to converge barotropic momentum into the jet (Stone 1969; Ioannou and Lindzen 1986). While some exceptions to this rule can be contrived (Held and Andrews 1983), the vast majority of examples support it. Enhancement of the background barotropic velocity has crucial implications for development of absolute instability because, due to the finite propagation speed of unstable pulses, a sufficiently strong barotropic velocity can transform an absolute instability into a convective instability. This fact opens the possibility that, in horizontally sheared flows, absolutely unstable eddies may be stabilized by enhancement of barotropic velocity in the jet core as an alternative to reduction of the baroclinic shear.

Since eddy momentum fluxes scale with the square of the wave amplitude, the acceleration of the barotropic jet is expected to be concentrated where the amplitude is largest, assuming perturbation velocity correlation persists at high amplitude. For asymptotically long times the response of an absolute instability approaches (3) in which the amplitude may increase in the x direction. The imaginary part of k_s in (3) as a function of the nondimensional barotropic velocity for two different horizontally uniform background states appropriate to midlatitudes is shown in Fig. 2. We see that U and the imaginary part of k_s are typically of opposite sign; that is, absolute instabilities generally grow in the direction of the barotropic velocity. Assuming that disturbances grow in the direction of U even in the presence of horizontal shear, an instability of sufficient amplitude could focus enough momentum into a jet to transform a locally absolutely unstable region into a convectively unstable region, and this transition would be likely to occur first in the downstream region. Further growth could then expand the newly formed convectively unstable region into the absolutely unstable regions. If, in addition, a minimum size to sustain local instability exists, then the instability could stabilize by creating locally convectively unstable regions downstream through momentum convergence so as to confine absolutely unstable regions to this minimum size.

Based on simplified models, Pedlosky (1989, 1992) has suggested that this critical size for existence of absolute instability may be a Rossby radius or smaller, but caution must be exercised in applying this result to our proposed equilibration mechanism because the assumptions made by Pedlosky and those made in this work are not exactly equivalent. We proceed by numerically determining the eigenmodes in a periodic two-layer model with a sponge layer. Full eigenanalysis of this model becomes unmanageable even for modest resolution. We chose the spectral expansion in Cai and Mak (1990) with 16 zonal wavenumbers and 10 meridional wavenumbers. Furthermore, we take advantage of the fact that the even and odd meridional components are decoupled for flows considered here and can be solved separately. Other details regarding the eigencalculation of this well-known model can be

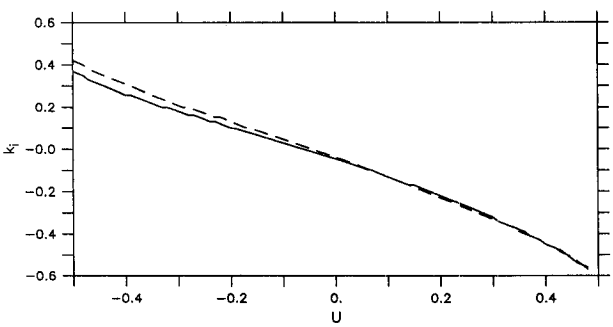

FIG. 2. The imaginary part of the wavenumber k_s [$k_i = \text{Im}(k_s)$] for absolute instability as a function of nondimensional barotropic velocity, U. The solid curve corresponds to the standard case $\beta = 0.4$; the dash corresponds to $\beta = 0.3$. Positive imaginary part of k_s represents a wave amplitude that grows in the $-x$ direction, while a negative imaginary part corresponds to a wave amplitude that grows in the $+x$ direction.

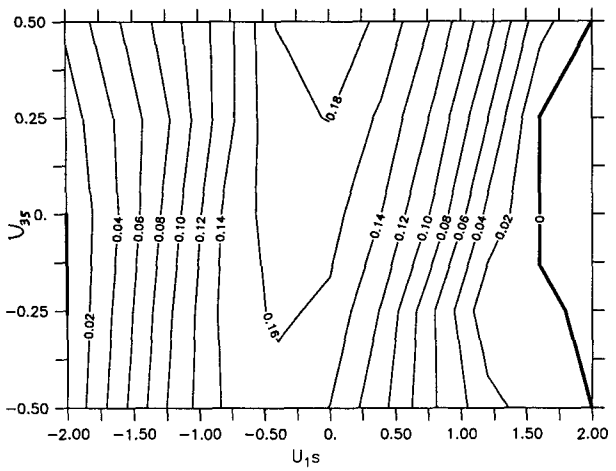

FIG. 3. Contours of the maximum growth rate of local instability in a baroclinic zonal jet of the form (9a, 9b) bounded zonally by a sponge. The standard parameter $\beta = 0.4$ is used and the channel extends 30 units in the zonal direction, and 6 in the meridional. The growth rates were calculated by a spectral eigenanalysis using 16 zonal wavenumbers and 10 meridional wavenumbers.

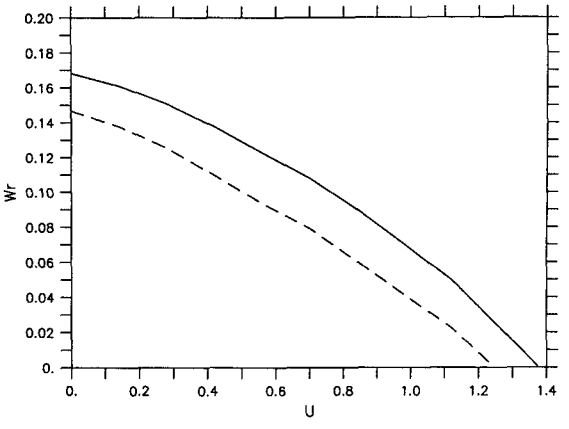

FIG. 4. Maximum growth rate, ω_r, of local instability in the baroclinic zonal flow (9c) for the case of no surface friction (solid) and the case with surface friction of magnitude $1/\tau_D = 0.1$ (dash). The standard parameters $\beta = 0.4$ and $l = 0.5$ are assumed.

found in Cai and Mak (1990). The basic state is first chosen to be a sine jet with velocities defined by

$$U(y) = U_{1s}\sin(\pi y/L_y) + U_{3s}\sin(3\pi y/L_y) \quad (9a)$$

$$H(y) = \sin(\pi y/L_y) \quad (9b)$$

and with a sponge given by

$$r(x) = \begin{cases} r_0 \exp\left[-\left(\dfrac{x}{b}\right)^2\right], & 0 < x < \dfrac{1}{2} \\ r_0 \exp\left[-\left(\dfrac{x-1}{b}\right)^2\right], & \dfrac{1}{2} < x < 1, \end{cases} \quad (10)$$

where $r_0 = 10$ (dimensional damping rate of 1/2500 sec^{-1}). The parameter b has to be chosen carefully: if b is too small, global modes will penetrate the sponge; if b is too large, the sponge encroaches on the wave domain and damps the disturbances. We chose $b = 0.3$. The maximum growth rate as a function of the first two odd sine modes of the barotropic velocity is shown in Fig. 3. The stability characteristics of the local modes are predominantly controlled by the largest meridional mode, so we hereafter consider the growth rate of local instabilities as a function of this gravest mode alone:

$$U(y) = U\sin(y\pi/L_y), \quad H(y) = \sin(y\pi/L_y). \quad (9c)$$

The growth rate as a function of U defined in (9c) is shown in Fig. 4. Note that the full 3D flow with horizontal shear requires an absolute instability cutoff velocity slightly less than $U = 1.4$, close to the value obtained analytically (6) for horizontally uniform flows. This correspondence suggests, at least for the simple jet structures considered here, that the stability of the flow is primarily determined by the local stability characteristics along the jet core. The addition of surface drag with damping rate $1/\tau_D$ shifts the growth rate curve downward so that the transition from absolute to convective instability occurs at less positive barotropic velocities, consistent with the results of Merkine and Shafranek (1980). The barotropic streamfunction for the most unstable mode at $U = 0.8$ is shown in Fig. 5. Two features previously discussed are clearly present: the wave amplitude grows rapidly in the direction of the barotropic velocity, and the phase tilt of the horizontal structures implies that the mode converges zonal momentum into the jet core. Since the dominant zonal wavenumber is 5 while the eigenanalysis is truncated at 16, we believe that the resolution of the eigenanalysis is sufficient.

Assuming that the mode illustrated in Fig. 5 maintains its general structure as it grows to large amplitude, it follows that the background barotropic jet will accelerate and that the downstream region will be first to transition from local absolute instability to local convective instability. Since the unstable waves are zonally bounded by the sponge, continued growth of the instability will cause the local convectively unstable regions to expand and the local absolutely unstable regions to contract. We therefore envision the equilibrated flow

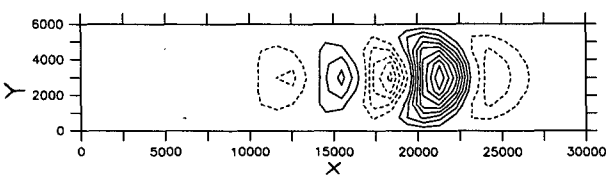

FIG. 5. Contours of barotropic streamfunction of the most unstable local instability for the case $U = 0.8$ defined in (9c), $\beta = 0.4$, $l = 0.5$, and $1/\tau_D = 0$. The distances are in kilometers.

to have a downstream region of local convective instability, an upstream region of local absolute instability, and a transition region somewhere in between. To investigate the stability properties of such a flow, we choose the following simple flow: the upstream velocity U_A and the downstream velocity U_C are chosen to be constant in x and the transition region, centered at x_c, is chosen to be a Rossby radius wide in which a sine-squared function smoothly joins the two flows. Explicitly,

$$U(x) = \begin{cases} U_A, & x < x_c - \frac{1}{2} \\ U_A + (U_C - U_A)\sin^2\left(\dfrac{\pi(x - (x_c - \frac{1}{2}))}{2}\right), & x_c - \frac{1}{2} < x < x_c + \frac{1}{2} \\ U_C, & x > x_c + \frac{1}{2}. \end{cases} \tag{11}$$

We multiply the zonally varying profile (11) by $\cos(\pi y/L_y)$ to obtain an analytic streamfunction such that (11) is the zonal profile along the central latitude along which the jet maximum is located. We determined the eigenvalues of the two-layer model based on this mean streamfunction and based on the sponge (10) using the spectral method described in Cai and Mak (1990). The eigenmodes are local instabilities of the flow and were verified to be independent of the sponge damping for $r_0 > 3$ (recall that we use $r_0 = 10$). The maximum growth rate of the eigenmodes based on this zonally varying streamfunction as a function of x_c is shown in Fig. 6 for the case $U_A = 1$, $U_C = 1.6$ (the dashed line will be explained shortly). We see that the flow is stable when the transition point x_c drops below 12. This confirms the possibility that local instabilities may be stabilized by restricting locally absolutely unstable regions below a critical zonal length.

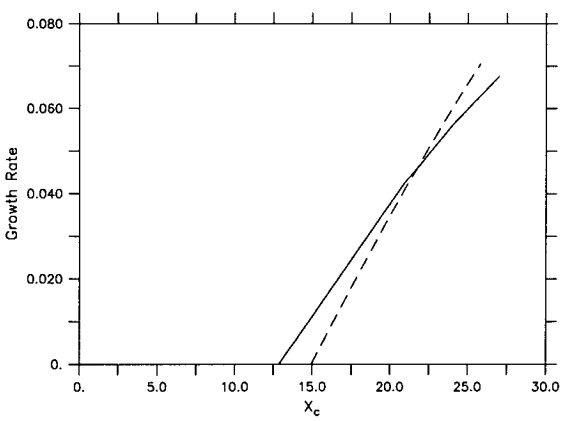

FIG. 6. The solid line is the maximum eigenmode growth rate of a flow locally absolutely unstable ($U_A = 1$) for $x < x_c$ and convectively unstable ($U_C = 1.6$) for $x > x_c$ for the 3D zonally varying flow discussed in the text. The dash curve corresponds to the maximum growth rate found in the 1D model with the same sponge and using the zonal velocity along the jet axis of the 3D flow.

Since the stability of the chosen 3D flow appears to be controlled by the local stability characteristics along the jet core, it may be useful to ignore the meridional variations and calculate the eigenmodes of a purely zonally varying flow to understand the results of the 3D eigenanalysis. Pierrehumbert (1984) also found this 1D model to be useful for understanding the wave propagation characteristics in zonally varying flows. Formally, the meridional velocities required to maintain mass balance of a zonally varying flow could be accounted for by a distribution of mass sources and sinks, which would not appear in the perturbation analysis. The use of this model is justified by the fact that it yields nearly the same zonal structure and growth rate of the absolute instabilities as does the full 3D model. The dynamical equations linearized about this purely one-dimensional state are

$$\frac{\partial q_n'}{\partial t} + U_n(x)\frac{\partial q_n'}{\partial x} + \frac{\partial \psi_n'}{\partial x}\left(\beta - \frac{\partial^2 U_n}{\partial y^2} - (-1)^n\right) = -r(x)q_n' \tag{12a}$$

$$q_n' = \nabla^2\psi_n' + (-1)^n(\psi_1' - \psi_2'), \quad n = 1, 2, \tag{12b}$$

where $U_n(x)$ is the nondimensional mean zonal velocity in the nth layer, $\psi_n'(x, y, t)$ is the perturbation streamfunction, and $r(x)$ is the damping coefficient. For the nondimensionalization we choose the reference Rossby radius to be 1000 km and the reference vertical shear to be the maximum radiative-equilibrium vertical shear, taken to be 20 m s^{-1} in all experiments. In these units, $\beta = 0.4$, and the channel is 6 units in meridional width and 30 units in zonal length. The growth rate as a function of x_c is shown as the dashed line in Fig. 6. The critical length for instability and the increase in growth rate as a function of x_c are nearly the same as in the 3D example if the advection velocities along the central latitude of the full 3D flow are used in the comparison. These results suggest that for local instability to exist, a region of absolute instability must exceed a critical size along the jet maximum that depends only

weakly on the magnitude of β and meridional shear (except near the cutoff speed). Setting $U_A = 1$, the maximum growth rate as a function of U_C and x_c is shown in Fig. 7. The contours stop at $x_c = 3$ and $x_c = 27$ because the sponge damping becomes important there. In other words, the transition point enters the sponge when $x_c < 3$, and the flow becomes locally convectively unstable everywhere outside the sponge in this case. In general, the critical size increases as the downstream velocity U_c of the convectively unstable region increases. Unfortunately, U_c cannot generally be predicted since it is determined by the nonlinear wave–mean flow interactions.

The critical size can be sensitive to the way the global modes are filtered. For "square well"–type sponges the critical size can be half that in the Gaussian sponge for the same U_C. As the sponge becomes smoother, the critical size increases, although it becomes increasingly difficult to define "sponge free." Nevertheless, the same qualitative behavior as indicated in Fig. 7 was found for all functions $r(x)$ that we tried.

We next study the dynamics of absolute instabilities as they evolve into the nonlinear regime. In the following sections, we describe our nonlinear model and examine the disturbances that develop and equilibrate in both absolutely and convectively unstable systems.

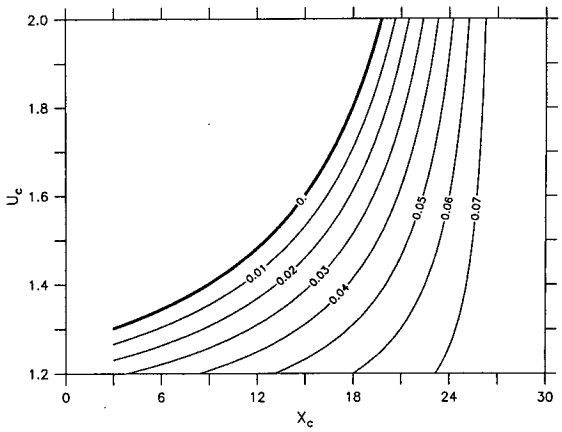

FIG. 7. Contours of local instability maximum growth rate of the one-dimensional zonally varying flow (11), which is locally absolutely unstable for $x < x_c$ and locally convectively unstable for $x > x_c$ and bounded in x by a sponge. The upstream velocity U_A is unity. The growth rates were found by an eigenanalysis using 64 zonal wavenumbers. The zonal length of the channel is 30 nondimensional units and standard parameters $\beta = 0.4$, $l = 0.5$ are assumed.

3. The model

We simulate the midlatitude troposphere with a radiatively driven quasigeostrophic two-layer model. Friction is parameterized as a momentum sink proportional to the velocity of the bottom layer with proportionality constant $1/\tau_D$. The radiative driving is simulated as a Newtonian damping of $\theta^*(y)$ with timescale τ_R. The model geometry is a periodic β plane with walls at $y = 0, L_y$. The full dimensional equations of motion are (Pedlosky 1987)

$$\frac{D_n}{Dt}(q_n) = 2(-1)^n\left(\frac{\theta^* - \theta}{L_R^2 \tau_R}\right) - r(x)(q_n - q_n^*) + \frac{\delta_{2n}}{\tau_D}\nabla^2\psi_2 \quad (13)$$

$$\frac{D_n}{Dt} \equiv \frac{\partial}{\partial t} + \frac{\partial \psi_n}{\partial x}\frac{\partial}{\partial y} - \frac{\partial \psi_n}{\partial y}\frac{\partial}{\partial x} \quad (14)$$

$$q_n = \nabla^2\psi_n + (-1)^n\frac{2\theta}{L_R^2} + \beta y, \quad (15)$$

where the subscript n identifies the top layer if $n = 1$ and the bottom if $n = 2$, δ_{2n} is 0 if $n = 1$ and is 1 if $n = 2$, ψ_n is the streamfunction for the velocity in the nth layer:

$$U_n = -\frac{\partial \psi_n}{\partial y}, \quad V_n = \frac{\partial \psi_n}{\partial x}, \quad (16)$$

and $\theta \equiv (\psi_1 - \psi_2)/2$ is proportional to the vertically averaged temperature. The asterisk denotes the prescribed flow fields that are chosen to control the absolute or convective nature of the basic flow.

The kinematic boundary condition of zero normal flow at the walls requires that the normal velocity vanish

$$v_n = \frac{\partial \psi_n}{\partial x} = 0 \quad (17)$$

everywhere along the walls located at $y = 0$ and $y = L_y$. This implies that ψ is at most a function of time along the wall, but a second condition is needed to determine this function of time. This extra condition is usually obtained by integrating the order Rossby number zonal momentum equations along the wall, making use of the fact that both the geostrophic and ageostrophic meridional velocities vanish at the walls. The result is

$$\frac{\partial}{\partial t}\int_0^{L_x}\frac{\partial \psi_n}{\partial y}\,dx = -\int_0^{L_x} r(x)\left(\frac{\partial \psi_n}{\partial y} - \frac{\partial \psi_n^*}{\partial y}\right)dx. \quad (18)$$

The vanishing of eddy fluxes at the walls, which was used to derive (18), implies that the net zonal velocity cannot change except in response to external forcing. The value of $r(x)$ inside the sponge is sufficiently large that the zonal velocity inside the sponge is strictly maintained at the prescribed flow. Thus, we simply use

$$\begin{aligned} \psi_n(t) &= C_n \quad \text{at } y = 0 \\ \psi_n(t) &= D_n \quad \text{at } y = L_y, \end{aligned} \quad (19)$$

where C_n and D_n are constants. The difference $\psi_n(0)$

$-\psi_n(L_y)$, which is proportional to the mean layer mass flux, and the differences $\psi_1(0) - \psi_2(0)$ and $\psi_1(L_y) - \psi_2(L_Y)$, which are proportional to the temperature at the walls, are prescribed by the sponge. The constants C_n and D_n are therefore determined up to an overall constant, which could change in time. Since this constant does not affect the dynamics, we choose it such that the barotropic streamfunction $\psi_1(0) + \psi_2(0)$ vanishes on the southern boundary. The constants C_n and D_n are set at the beginning of each model run to be consistent with the chosen sponge.

Our standard parameter values were chosen to model the midlatitude troposphere:

$$\beta = 1.6 \times 10^{-8}\ \text{km}^{-1}\ \text{s}^{-1},$$

$$\tau_R = 20\ \text{days}, \quad L_x = 30\,000\ \text{km}$$

$$L_R = 1000\ \text{km}, \quad \tau_D = 5\ \text{days}, \quad L_y = 6000\ \text{km}.$$

The gridpoint model resolves the x direction with 64 points and the y with 17 points. The prescribed flow fields are of the form:

$$\psi_n^*(y) \equiv \Psi_n^* \cos(\pi y/L_y) \tag{20}$$

with $\frac{1}{2}(\psi_1^* - \psi_2^*) = \theta^*$, which is proportional to the radiative-equilibrium temperature, chosen to yield a maximum thermal wind $\frac{1}{2}(U_1 - U_2) = -d\theta^*/dy$ of 20 m s^{-1}. The nondimensional velocity of the prescribed flow field is independent of y and given by

$$U = \frac{\Psi_1^* + \Psi_2^*}{\Psi_1^* - \Psi_2^*}. \tag{21}$$

In the following numerical experiments, the difference $\Psi_1^* - \Psi_2^*$ is held constant so that the prescribed flow fields are completely specified by U, which is varied to control the velocities within the sponge. The streamfunction is related to the perturbation geopotential height, Φ, by $\psi = \Phi/f_0$, and to the vertically averaged temperature by the hypsometric equation $T = 2f_0\theta/R \approx (0.7\ \text{K s km}^{-2})\theta$. These relations require a temperature difference between the walls at radiative equilibrium of 53 K, which corresponds to a global average temperature gradient of 0.9 K/100 km. The criterion for inviscid instability for horizontally uniform flows at these parameter values is $U_1 - U_2 > 16$ m s^{-1}, and the most unstable mode is $l = 1$, $k = 4$, where l refers to the meridional wavenumber and k to the zonal wavenumber. All integrations were extended to 350 days.

4. Convective instabilities

We first consider the case in which the Gaussian sponge maintains a convectively unstable flow with $U = 1.6$ (recall that $U > 1.4$ is the approximate criterion for convective instability). We initialize the total flow with this velocity and a Gaussian-shaped perturbation in streamfunction with a half-width of three Rossby radii (the evolution for long times was verified to be independent of the initial perturbation). We define "perturbation" as deviations from the flow forced by the sponge layer.

As revealed in Fig. 8, the growing wave packets in a convectively unstable system propagate entirely downstream in the nonlinear simulation. Without a means of sustaining the eddy energy, the convectively unstable system ultimately obtains its thermally and frictionally forced, zonally symmetric steady state. This state is a baroclinic jet with maximum dimensional shear of 20 m s^{-1}, which exceeds the inviscid critical shear for instability by a factor of 2.5, yet no eddy exists after 20 days. This final state stands in stark contrast to the state without a sponge layer in which eddies persist indefinitely.

We have also examined convectively unstable eddies when the sponge damping is as large as $r_0 = 50$. In this case, illustrated in Fig. 9, the waves strongly reflect off the sponge, but the reflection of wave energy does not lead to unstable growth of eddies. We conclude that nonlinear, convectively unstable systems bounded by dissipative regions sufficiently strong to damp out global modes do not support instability.

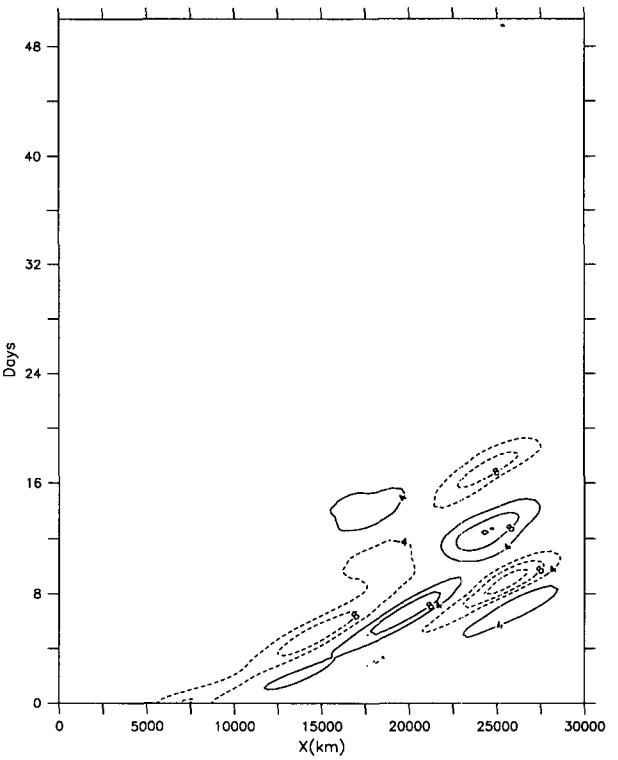

FIG. 8. Hovmöller diagram of eddy barotropic streamfunction along the central latitude (y = 3000 km) as a function of zonal distance and time for the nonlinear simulation in which the sponge relaxes to the convectively unstable flow $U = 1.6$. The sponge damps the initial and final 3000 km of the channel. "Eddy" refers to deviations from the value forced by the sponge, and the units of eddy streamfunction are km^2 s^{-1}.

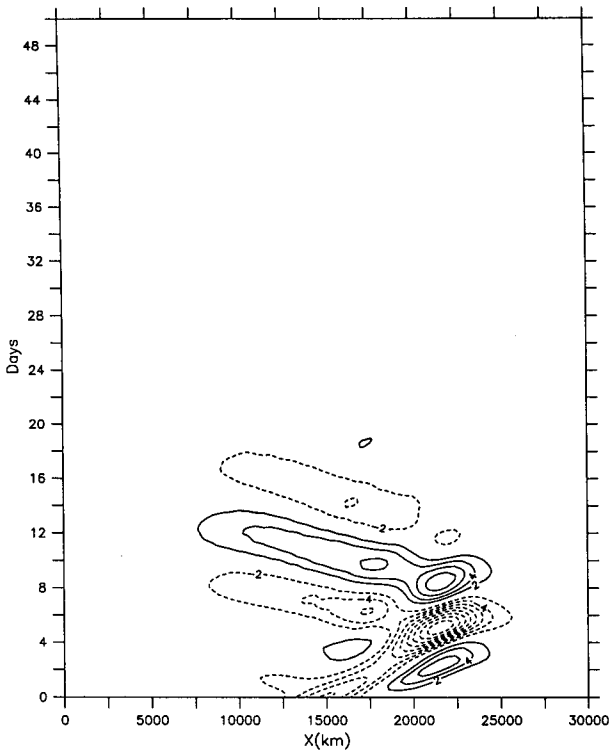

FIG. 9. Hovmöller diagram of eddy barotropic streamfunction along the central latitude (y = 3000 km) as a function of zonal distance and time for the nonlinear simulation in which the sponge relaxes to the convectively unstable flow U = 1.6, as in Fig. 8 except the sponge damping is five times larger (r_0 = 50). Units of eddy streamfunction are km^2 s^{-1}.

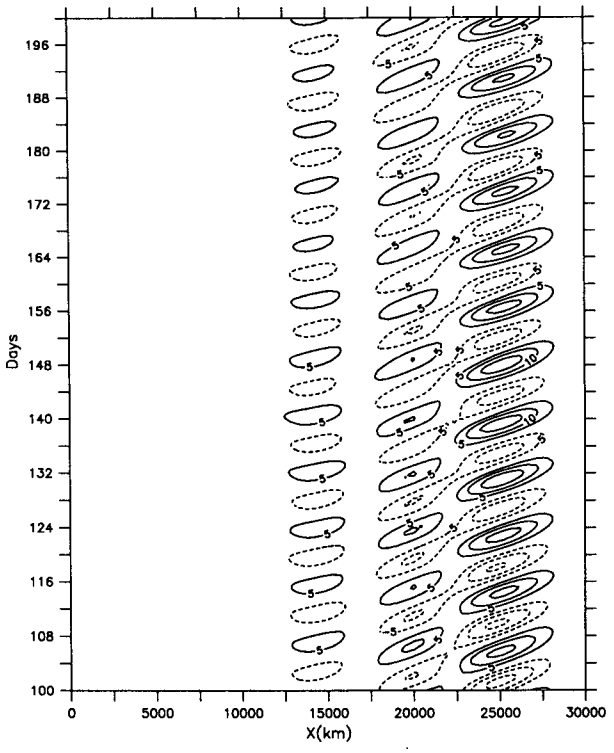

FIG. 10. Hovmöller diagram of eddy barotropic streamfunction along the central latitude (y = 3000 km) as a function of zonal distance and time for the nonlinear simulation in which the sponge relaxes to the absolutely unstable flow U = 1.0. Eddy streamfunction units are km^2 s^{-1}.

5. Absolute instabilities

We now consider the case in which the sponge layer forces the mean flow toward absolute instability. In this case, U = 1 and the perturbations remain beyond 30 days, as evidenced by the Hovmöller diagram for the original Gaussian sponge r_0 = 10 in Fig. 10. Perhaps the most remarkable feature of the evolution is that the perturbations oscillate regularly with a period of 8.4 days throughout the integration period. The frequency spectra for the point x = 25 000 km is shown in Fig. 11. The same sharp peak at 8.4 days was found at other regions of the flow. This period is not the period of the marginal instability, which is 4.1 days as determined by the three-dimensional eigenvalue analysis. The secondary peaks at 2.9 days and 4.1 days depend on the type of sponge and the size of the domain and therefore do not indicate robust features of the simulation. The mean zonal velocity averaged over the last 200 days of the simulation is shown in Fig. 12 and reveals the predicted enhancement of velocity in the downstream region.

Since our proposed mechanism requires a zonal barotropic velocity less than approximately U = 1.4 for the existence of linear absolute instability, it is important to verify that this condition also applies in the nonlinear regime. This question is especially relevant in light of the study by Lee and Held (1991), which showed that temporal instability in the two-layer model exhibits subcritical instability and hysteresis near the linear stability boundary. This phenomenon could negate the equilibration mechanism proposed here since it is assumed that disturbances are not self-maintaining when an absolutely unstable system is carried through

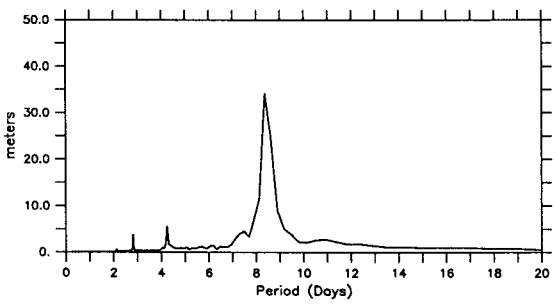

FIG. 11. Period spectra of the upper-layer rms geopotential height (in meters) at the point x = 25 000 km, y = 3000 km for the nonlinear simulation in which the sponge relaxes to the absolutely unstable flow U = 1. The spectral resolution near the peak at 8.4 days is $\pm 1/3$ day.

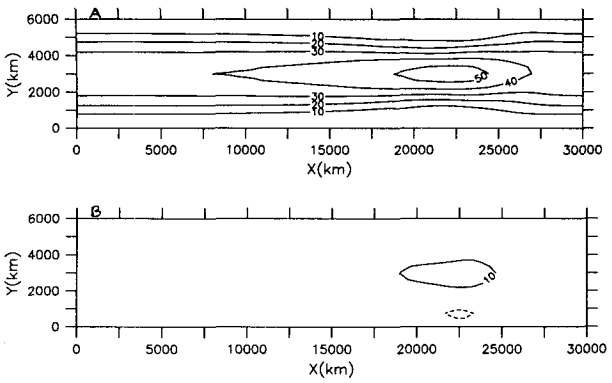

FIG. 12. Upper-layer (a) and lower-layer (b) zonal velocity averaged over the last 200 days of a 350-day nonlinear simulation in which the sponge relaxes to the absolutely unstable flow $U = 1$ (in dimensional units: $U_1 = 40$ m s^{-1}, $U_2 = 0$).

the transition into the convectively unstable regime by varying U. To explore this transition, we allow an absolute instability ($U = 1.0$) to equilibrate for 150 days, and at the 150-day mark we discontinuously change the sponge to force a convectively unstable flow ($U = 1.6$). The result of this experiment is depicted in a Hovmöller diagram (Fig. 13). It can be seen that the waves acquire a positive group velocity after 150 days and propagate into the sponge where they are ultimately absorbed. An extensive search through other regions of parameter space failed to reveal an example of eddies persisting in the convectively unstable regime. Thus, for a given baroclinic shear we find that the transition from absolute to convective instability depends primarily on the barotropic velocity along the jet maximum and occurs at approximately the same barotropic velocity in both the linear and nonlinear regimes; no hysteresis of absolute instability exists with respect to the barotropic velocity.

The upper-layer root-mean-square eddy geopotential height is shown in Fig. 14. This rms height is clearly localized in the extreme downstream side of the channel with a maximum of 165 m, about twice that observed in the storm tracks (Blackmon et al. 1977). The rapid increase in variance in the downstream direction is consistent with the Hovmöller diagram of the geopotential shown previously and is suggestive of exponential spatial growth characteristic of locally forced convective instabilities. It is clear that this disturbance would have propagated beyond the sponge to establish a global mode if the sponge did not exist; in other words, the disturbance is localized by the sponge. The rms height at other frequencies is small (see Fig. 11). This lack of variability on other timescales contrasts with the atmospheric fluctuations in which most of the variance occurs with periods larger than 10 days (Blackmon et al. 1977). The 200-day mean geopotential height reveals that the barotropic zonal velocities are stronger on the downstream side than on the upstream side. This downstream acceleration is primarily barotropic as the baroclinic shear is only weakly reduced, as shown in Fig. 15.

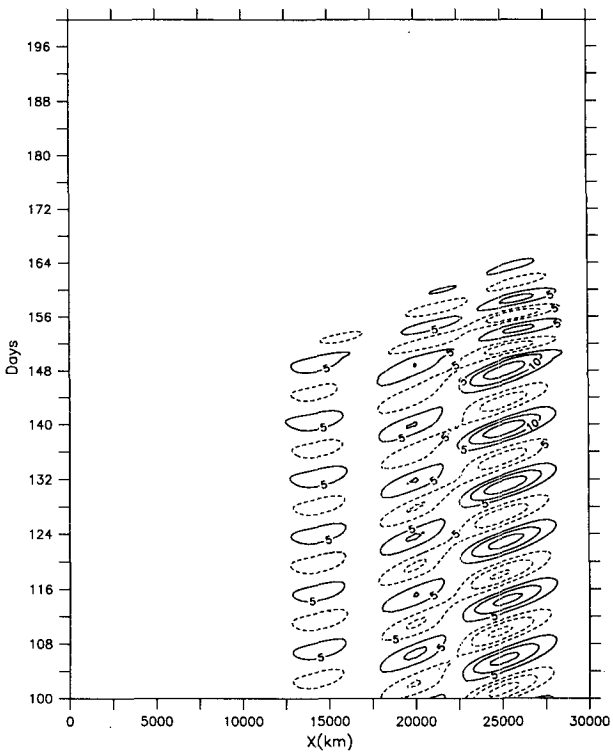

FIG. 13. Hovmöller diagram of the barotropic streamfunction for a single nonlinear simulation with the sponge relaxing to $U = 1$ (absolutely unstable) for the first 150 days and to $U = 1.6$ (convectively unstable) for the last 50 days of a 200-day simulation. Only the last 100 days are shown.

To determine whether the background state becomes convectively unstable in the downstream region, we show the time-mean nondimensional velocity U in Fig. 16 and the Hovmöller diagram for U in Fig. 17. The solid contours in Fig. 17 represent absolutely unstable regions ($U < 1.4$), while the dashed lines represent convectively unstable regions ($U > 1.4$). The zonal flow is seen to develop convectively unstable regions just large enough to limit the region of absolute instability to its critical size. The transition from local absolute instability to local convective instability

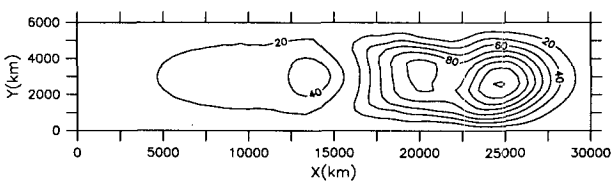

FIG. 14a. Contours of rms eddy geopotential height (in meters) of a nonlinear simulation in which the sponge relaxes to the absolutely unstable flow $U = 1$. The contour interval is 20 m.

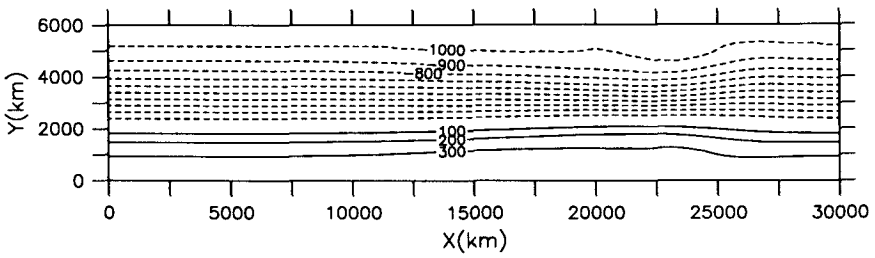

FIG. 14b. Contours of the time-mean upper-layer geopotential height (in meters) of a nonlinear simulation in which the sponge relaxes to the absolutely unstable flow $U = 1$. The contour interval is 20 m.

(marked by $U = 1.4$) averages about 18 000 km, not far from the transition $x_c = 17\,000$ implied by Fig. 3 based on a maximum downstream velocity of $U_C = 1.8$ (that the choice $U_C = 1.8$ is appropriate can be seen from examination of Fig. 16). We expect the nonlinearly equilibrated size of the absolutely unstable region to exceed that required for stability because the flow must be slightly unstable in order for eddies to persist. The damping influence of the sponge can be estimated from the previous figures to be confined to 3000 km on each end of the channel. Therefore, the absolutely unstable region occupies the zonal length 17 000 − 3000 = 14 000 km. If we assume that the downstream velocity is at least $U_C = 1.6$ for all parameter values, Fig. 3 suggests that the critical length of the locally absolutely unstable region (minus the sponge) is 9000 km. This zonal distance is thus the minimum critical distance an absolutely unstable region must span in order for local instability to exist. When we doubled the length of the channel to 60 000 km (and doubled the sponge damping to $r_0 = 20$), the equilibrated flow contained an absolutely unstable region spanning 12 000 km (with the sponge subtracted out). Thus, the minimum size 9000 km is well approximated by our linear calculations and is relatively independent of the length of the channel.

We have examined the response for a wide variety of parameter values to test the generality of this equilibration mechanism. As the frictional and radiative damping is reduced, the disturbances become more irregular in time but the total size of local absolutely unstable regions never contract smaller than the minimum size of 9000 km (based on $U_C = 1.6$) independent of the value of beta and the Rossby radius. The results in which the eddies are regular are summarized in Table 1, where "marginal mode" refers to the flow specified by (11) with $U_C = 1.6$. The discrepancy between the critical x_c based on the marginal mode and that based on the equilibrated flow is due to the fact that the velocities produced in the downstream convectively unstable regions exceed the chosen downstream speed of $U_C = 1.6$ assumed in (11). Consider, for instance, the case in which beta is reduced to 1/4 its standard value. For $U_C = 1.6$ in (11), the linear calculations yield a critical size around 5000. In the nonlinear equilibration, the size is 9500 km. The time-averaged zonal velocity along the central latitude, shown in Fig. 18, reveals that the increase in barotropic velocity and the reduction of vertical shear play equally important roles in the equilibration to yield a much larger downstream value of U/H. The eddies in this example and for most of the other parameter values are more irregular than are those found for the standard parameters. When U_C in (11) is

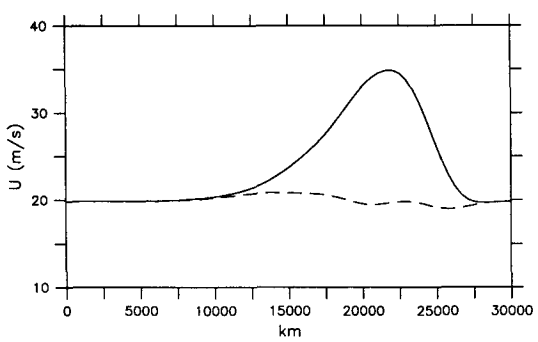

FIG. 15. Dimensional barotropic velocity $(U_1 + U_2)/2$ (solid) and baroclinic velocity $(U_1 - U_2)/2$ (dashed) along the central latitude $y = 3000$ km of a nonlinear simulation in which the sponge relaxes to the absolutely unstable flow $U = 1$. The velocities have been averaged over the last 200 days of a 350-day nonlinear simulation.

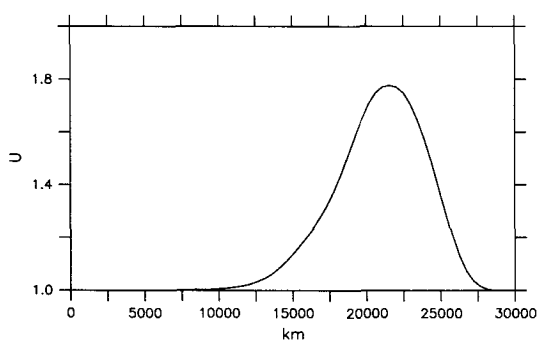

FIG. 16. Nondimensional velocity U along the central latitude $y = 3000$ km corresponding to Fig. 15 in which the sponge relaxes to the absolutely unstable flow $U = 1$.

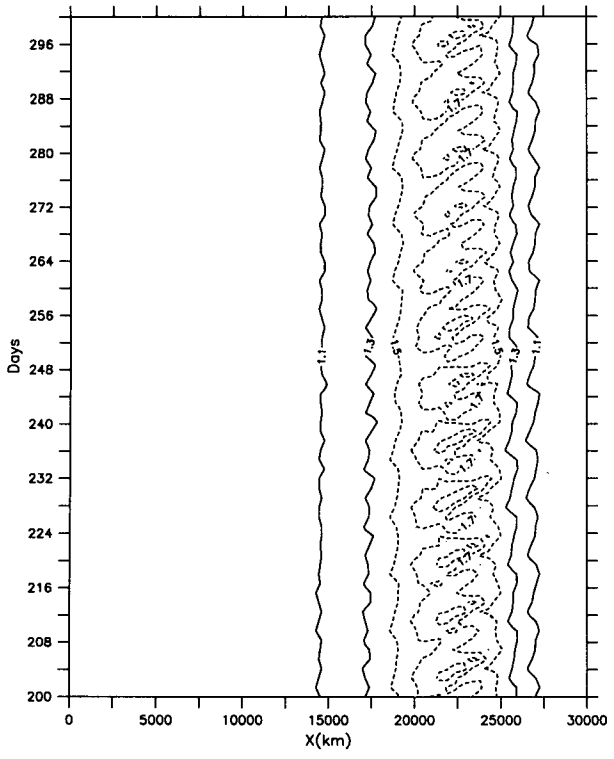

FIG. 17. Hovmöller diagram of the nondimensional velocity U along the central latitude (y = 3000 km) of the channel of a nonlinear simulation in which the sponge relaxes to the absolutely unstable flow $U = 1$.

TABLE 1. Equilibration properties of absolute instabilities.

	Nonlinear results			Linear marginal mode	
Case	Max U_c	Length of AU region (km)	Dominant period (d)	Critical size (km)	Period (d)
standard	1.8	15 000	8.4	11 000	4.1
$\beta_0/2$	2.3	10 800	6.2	2 000	3.5
$\beta_0/4$	3.0	9 600	4.6	5 000	3.1
$\tau_D = 0$	1.6	9 200	15.8	10 500	4.1
$2L_x$	1.6	12 000	10.0	20 000	4.7

$$\sum_{n=1}^{2}\left(\frac{\partial \epsilon_n}{\partial t} = -U_n\frac{\partial \epsilon_n}{\partial x} + \nabla\cdot\mathbf{S}_n - U_n\frac{\partial}{\partial y}\left(\frac{\partial \psi_n}{\partial y}\frac{\partial \psi_n}{\partial x}\right) + \frac{\lambda^2}{2}H\theta\frac{\partial}{\partial x}(\psi_1+\psi_2)\right). \quad (22)$$

$$\epsilon_n = \frac{1}{2}\left(\frac{\partial \psi_n^2}{\partial x} + \frac{\partial \psi_n^2}{\partial y} + \frac{\lambda^2}{2}\theta^2\right) \quad (23)$$

$$S_{x,n} = \psi_n\frac{\partial^2\psi_n}{\partial x\partial t} + U_n\psi_n\frac{\partial^2\psi_n}{\partial x^2} + \frac{U_n}{2}\frac{\partial^2\psi_n^2}{\partial y^2} + \frac{1}{2}\psi_n^2\left(\beta - \frac{\partial^2 U_n}{\partial y^2}\right) \quad (24)$$

$$S_{y,n} = \psi_n\frac{\partial^2\psi_n}{\partial y\partial t}, \quad (25)$$

chosen to be 3, as Fig. 18 suggests for this parameter case, the linear calculation gives 9000 km for this critical extent. Thus, it appears that our equilibration mechanism operates in this case also, but the modes are able to transport more heat than the modes found at our standard parameters. This is perhaps not surprising when we consider the fact that the ambient shear is 10 times larger than the critical shear, a supercriticality never achieved in the atmosphere.

6. The role of local absolute instabilities

Figures 12 and 13 reveal that the disturbances are of relatively small amplitude inside the absolutely unstable region, and the question arises as to whether this region determines the spatial and temporal characteristics of the equilibrated disturbances or acts simply as a weak source of excitation, which "seeds" the downstream eddies. The eddy energy budget provides some insight into this issue. We ignore Newtonian cooling and surface friction because they are small compared to the other terms. Taking the mean flow to be the zonal mean velocity U_n, it is a routine procedure to derive the following dimensional eddy energy equation:

where $S_{x,n}$ and $S_{y,n}$ are the x and y components of S, respectively. Friction and radiative damping terms are negligible in the region bounded by the sponge and are ignored. We call the first term on the right-hand side of (22) the geostrophic advection term, the second the flux convergence term, the third the barotropic conversion term, and the last the baroclinic conversion term.

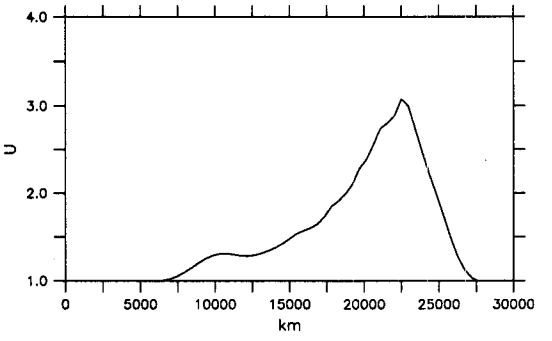

FIG. 18. Nondimensional zonal velocity as a function of x along the central latitude (y = 3000 km) in which the sponge relaxes to the absolutely unstable flow $U = 1$, as in Fig. 16 but with $\beta = 0.1$ instead of the standard $\beta = 0.4$. The zonal velocity shown is the average over the last 200 days of a 350-day nonlinear simulation.

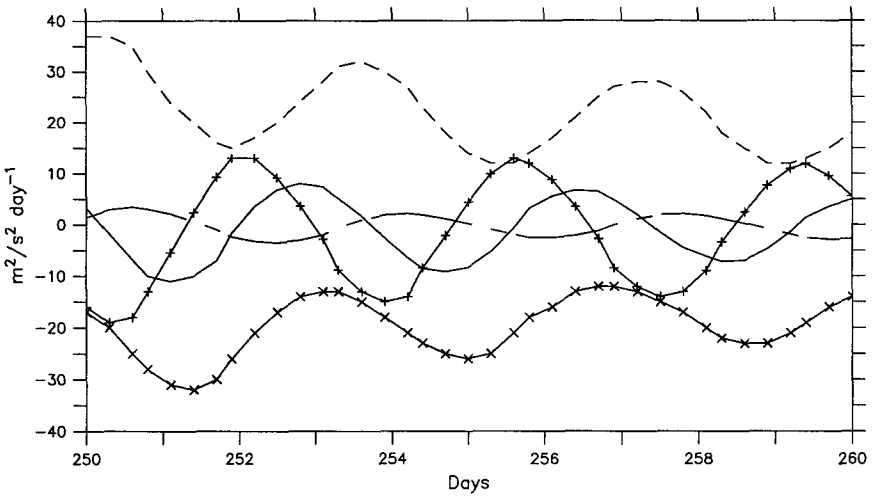

FIG. 19. Time series of the volume-averaged energy generation rate (solid), baroclinic conversion generation rate (dashed), barotropic conversion rate (long dashed), geostrophic flux convergence (solid ×), and ageostrophic flux convergence (solid +) of a nonlinear simulation in which the sponge relaxes to the absolutely unstable flow $U = 1$. Units are in $m^2\ s^{-2}\ day^{-1}$.

Note that only the last two terms of (22) contribute to the global average eddy energy—the first two merely redistribute eddy energy.

A time series of the four sources (and the time rate of change of energy) for a box 3000 km in zonal length and stretching from wall to wall is shown in Fig. 19. This time series is typical of that for any similar box away from the sponges. The eddy energy budget is characterized by 1) a source from baroclinic conversion, 2) a sink from geostrophic advection of eddy energy, 3) a negligible contribution from barotropic conversion, and 4) a source from ageostrophic flux convergence during the initial stages of eddy growth that becomes a sink during the latter stages of growth. (Although geostrophic advection acts as a sink away from the sponges, it acts as a source in a small region near the sponge with an amplitude just large enough to yield vanishing net eddy energy generation by geostrophic advection alone.) The frequency of oscillation between the growth and decay phase is $1/3.7\ day^{-1}$, or about twice the frequency of ψ, as expected since energy is quadratic in ψ.

The equilibration of the absolute instabilities as revealed by these energetics is quite different from the equilibration of normal modes in a periodic domain. If a balanced zonal flow on a sphere is perturbed by a small-amplitude normal-mode instability, the disturbances grow baroclinically into the nonlinear regime and subsequently decay barotropically (Simmons and Hoskins 1978). In our simulations, barotropic conversion is relatively unimportant (although necessary for the equilibration mechanism itself). In addition, disturbance growth and decay are preceded by substantial energy flux convergence and divergence, respectively. Because the eddy amplitude grows in the downstream direction, the geostrophic advection term is of single sign. In contrast to the classic development of baroclinic waves, baroclinic conversion peaks only during the late stages of eddy growth.

This energy budget is similar to that found downstream of localized initial perturbations (Simmons and Hoskins 1979; Orlanski and Chang 1993). In these cases, the disturbance first enters the domain of study (which is assumed fixed in space) and grows by advection (which includes geostrophic advection and ageostrophic flux convergence) at a rate 2–3 times larger than the growth rate of the most unstable wave. As the wave packet fills the domain, the perturbation growth by advection decreases, while that by baroclinic conversion increases. If the system is absolutely unstable, the baroclinic conversion ultimately dominates the energy growth; if the system is convectively unstable, the packet leaves the domain of study, signaled by a decrease due to advection of perturbation energy, and the perturbation energy vanishes asymptotically. In general, the baroclinic conversion dominates only after the net growth rate has peaked. In our model, the energetics of the downstream convectively unstable region is precisely that just described for an isolated wave packet except that instead of a single localized perturbation, a new perturbation is apparently excited every 8.4 days. That disturbances in the middle and downstream section grow by the same mechanism as do disturbances that receive their energy from an upstream source of perturbations suggests that the region of absolute instability serves primarily as a generator of perturbations, which subsequently grow downstream.

We caution that similarity between observations and our numerical simulations is not grounds for believing that local instabilities exist in the atmosphere. In par-

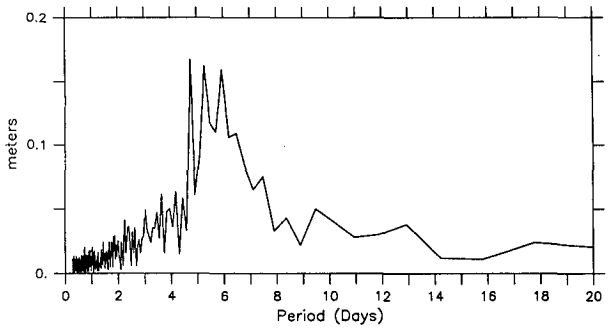

FIG. 20. Period spectra of the rms geopotential height (in meters) of the stochastically forced potential vorticity Eq. (13). The forcing region is $0 < x < 10\,000$ km, the sponge relaxes to the convectively unstable velocity $U = 1.6$, and the spectrum is taken from a time series of the upper-layer geopotential height at the point $x = 22\,500$ km, $y = 3000$ km.

ticular, an energetic analysis of transient disturbances in *stable* systems studied by Farrell (1984), which closely resembles the Type B cyclogenesis mechanism discussed by Petterssen and Smebye (1971), would yield essentially the same sequence of events: initial growth by geostrophic or ageostrophic advection (the upper-level trough enters the domain), baroclinic conversion dominates eddy growth for a period (the upper-level trough interacts with a low-level depression and develops into a cyclone), the eddy decays by geostrophic and ageostrophic advection (the weakened cyclone exists the domain). Depending on the initial condition and basic state, a wide variety of other life cycles can be explored where friction, barotropic conversion, and latent heat release also play important roles (Montgomery and Farrell 1990, 1991, 1992, 1993).

A remarkable aspect of the equilibration of absolute instabilities in our model is the sharply peaked frequency response (50% of the variance is located at periods 8.4 ± 1.8 d). Furthermore, this period is nearly double that predicted for the period of the marginal instability. This discrepancy suggests that something other than an unstable normal mode determines the frequency response of the equilibrated disturbances. The frequency of the marginally unstable mode for various parameter values is summarized in Table 1 along with the results of the nonlinear simulations. Typically, the period of the marginal mode is 20%–85% less than the frequency of the equilibrated disturbances.

We believe the frequency peak is associated with vacillation of the mean flow and not with the frequency of the absolute instability itself. Consider the following proposed sequence of events causing the downstream zonal flow to vary in time: the convectively unstable region grows as the unstable waves accelerate the barotropic jet until absolute instability is extinguished, but once the waves decay, the steady westerly flow from the sponge advects downstream, once again extending the absolutely unstable region. This advection eventually destabilizes the system, leading to excitation of downstream eddies. The process repeats when the downstream eddies grow large enough to once again accelerate the barotropic jet. Such an alternation produced by the eddies and momentum advection from the sponge would induce a periodicity of the basic flow with a frequency not directly related to the frequency of instability. To quantitatively estimate this frequency requires solving the perturbation equations with time periodic coefficients, solving for the wave–mean flow feedback on the barotropic velocity, and finding a self-consistent solution for the frequency and wave structures. Due to the complexity of this analysis we have not attempted an explicit verification of this mechanism.

Some final points can be made regarding the equilibration of absolute instability in the model. A three-dimensional eigenvalue analysis of the equilibrated flow averaged over the last 200 days indicates that this flow is stable. This result verifies that the flow equilibrates by rendering the basic state stable by wave–mean flow interactions. Now consider the following experiment. Start with the convectively unstable flow and stochastically add and subtract potential vorticity at each grid point in the region $0 < x < 10\,000$ km in the channel. Operationally, this can be done by introducing a random forcing on the right-hand side of (10). The purpose of this experiment is to determine whether the system possesses a linear response intrinsically peaked at 8.4 days. For convenience, the random numbers were chosen uniformly between $q' = \pm 10^{-6}\ \mathrm{s}^{-1}$. The resulting rms geopotential height spectrum at $x = 22\,500$ km is shown in Fig. 20. It is clear that disturbances with periods between 4 and 8 days are more strongly excited than those around 8.4 days. The resulting spectrum due to forcing the same region stochastically in time but limited to sines and cosines with zonal wavenumber 3, meridional wave-

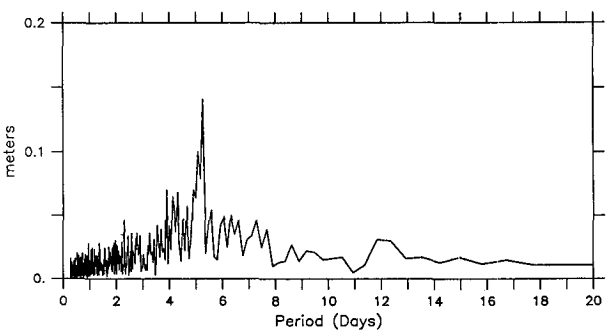

FIG. 21. Period spectra of the rms geopotential height (in meters) of the stochastically forced potential vorticity Eq. (13), as in Fig. 20 but the forcing is applied only to the spatial distributions $\sin(3x)\sin(y)$ and $\cos(3x)\sin(y)$ in the region $0 < x < 10\,000$ km. As in Fig. 20, the sponge relaxes to the convectively unstable flow $U = 1.6$ and the spectrum is taken from a time series of the upper-layer geopotential height at the point $x = 22\,500$ km, $y = 3000$ km.

number 1 is shown in Fig. 21. This forcing was chosen to simulate the scale of perturbations found in the nonlinearly equilibrated flow (see Fig. 11). The variance is sharply peaked around 5.4 days, the period of the marginal absolute instability, and relatively small near 8.4 days. That the variance of the nonlinear disturbances is largest downstream from the region of absolute instability suggests that the absolutely unstable region immediately after the sponge serves primarily to generate perturbations, which subsequently amplify as they propagate downstream. This leaves little doubt that the frequency of oscillation of the equilibrated eddies is not directly related to the frequency of the marginal instabilities or to the frequency of any other natural linear response of the system.

7. Summary and discussion

Synoptic activity on the 2–6-day timescale is concentrated in the oceanic storm tracks, and the explanation for this localization has been sought from a variety of theoretical perspectives. One suggestion has been that the storm tracks are absolutely unstable, enabling baroclinically unstable waves to remain in the local region of instability as the waves grow. In this paper we report how this linear theory extends into the nonlinear regime and the mechanisms by which the exponential growth predicted by linear theory is equilibrated at finite amplitude.

We use a sponge layer to inhibit recirculation of waves and to localize instabilities. We do not believe a dissipative sponge that damps out all waves actually exists in the atmosphere. It is well known, however, that synoptic-scale waves do not recirculate about the globe in a phase coherent manner, whereas eddies in periodic channel models exhibit a high degree of global coherence. We do not wish to discuss the factors that inhibit recirculation in the atmosphere because they appear to differ from case to case. The sponge is regarded as a modeling device that inhibits recirculation of synoptic-scale eddies and may or may not have a unique counterpart in the real atmosphere.

We found that an absolute instability converges momentum in such a way as to accelerate barotropic jets and that for sufficiently strong barotropic jets the downstream absolutely unstable regions became convectively unstable. Because the amplitude of absolute instability tends to grow in the direction of the barotropic velocity, we expected the transition from absolute to convective instability to occur first in the downstream region. As the unstable disturbance grows, the newly created convectively unstable region encroaches upon the absolutely unstable region. Linear calculations revealed that the system stabilizes when the absolutely unstable region becomes restricted to less than 9000 km for mean flows and parameter values appropriate to midlatitudes.

The transition from absolute to convective instability predicted by linear theory is found to be robust in the two-layer model, even when reflections from the sponge occur. That hysteresis of instability about the transition point was not found suggests that the instability criterion holds even in the nonlinear regime. Disturbances are self-maintaining only when the flow is absolutely unstable over sufficiently large zonal regions. The equilibration mechanism described above is verified to occur for a wide range of parameter values. The equilibrated disturbances are found to be most active in the convectively unstable region downstream of the absolutely unstable region, not in the region of absolute instability itself. Therefore, disturbances do not localize in regions of absolute instability if the downstream regions are convectively unstable.

If absolutely unstable storm tracks existed in the atmosphere, these results suggest that convectively unstable regions would develop in the downstream side of the oceanic jet maxima and would exhibit larger height variance there than in the absolutely unstable regions themselves. Moreover, these results suggest that the absolutely unstable regions must extend at least 9000 km in order to support local instability. It remains to be determined whether the equilibration mechanism found in our two-layer model also operates in vertically resolved models. The implication of our results to storm track dynamics, however, is that absolute instabilities need to overcome a highly restrictive requirement involving the extent of the domain in order to operate.

Acknowledgments. T. DelSole was supported by the NASA Global Change Graduate Fellowship. Brian Farrell was supported by NSF ATM-9216813. Brian Farrell was also partially funded by the US Department of Energy's (DOE) National Institute for Global Environmental Change (NIGEC) through the NIGEC Northeast Regional Center at Harvard University. (DOE Cooperative Agreement DE-FC03-90ER61010.) Financial support does not constitute an endorsement by DOE of the views expressed in this article/report. T. DelSole would like to thank R. Pierrehumbert and K. Swanson for engaging discussions on the physics of equilibration.

REFERENCES

Blackmon, M. L., J. M. Wallace, N.-C. Lau, and S. L. Mullen, 1977: An observational study of the Northern Hemisphere wintertime circulation. *J. Atmos. Sci.*, **34,** 1040–1053.

Briggs, R. J., 1964: *Electron–Stream Interaction with Plasmas.* The MIT Press, 8–46.

Cai, M., and M. Mak, 1990: On the basic dynamics of regional cyclogenesis. *J. Atmos. Sci.*, **47,** 1417–1442.

Farrell, B. F., 1982: Pulse asymptotics of the Charney baroclinic instability problem. *J. Atmos. Sci.*, **39,** 507–517.

——, 1983: Pulse asymptotics of three-dimensional baroclinic waves. *J. Atmos. Sci.*, **40,** 2202–2210.

——, 1984: Modal and nonmodal baroclinic waves. *J. Atmos. Sci.*, **41,** 668–673.

Hoskins, B., and B. J. Valdes, 1990: On the existence of storm tracks. *J. Atmos. Sci.*, **47,** 1854–1864.

Ioannou, P., and R. S. Lindzen, 1986: Baroclinic instability in the presence of baroclinic jets. *J. Atmos. Sci.*, **43,** 2999–3014.

Lee, S., and I. M. Held, 1991: Subcritical instability and hysteresis in a two layer model. *J. Atmos. Sci.*, **48,** 1071–1077.

Lin, S. J., and R. T. Pierrehumbert, 1993: Is the midlatitude zonal flow absolutely unstable? *J. Atmos. Sci.*, **50,** 505–517.

Lindzen, R. S., B. Farrell, and A. J. Rosenthal, 1983: Absolute barotropic instability and monsoon depressions. *J. Atmos. Sci.*, **40,** 1178–1184.

Montgomery, M. T., and B. F. Farrell, 1990: Dry surface frontogenesis arising from interior potential vorticity perturbations in a semigeostrophic model. *J. Atmos. Sci.*, **47,** 2837–2852.

——, and ——, 1991: Moist surface frontogenesis associated with interior potential vorticity anomalies in a semigeostrophic model. *J. Atmos. Sci.*, **48,** 343–367.

——, and ——, 1992: Polar low dynamics. *J. Atmos. Sci.*, **49,** 2484–2505.

——, and ——, 1993: Tropical cyclone formation. *J. Atmos. Sci.*, **50,** 285–310.

Merkine, L., 1977: Convective and absolute instabilities of baroclinic eddies. *Geophys. Astrophys. Fluid Dyn.*, **9,** 129–157.

——, and M. Shafranek, 1980: The spatial and temporal evolution of localized unstable baroclinic disturbances. *Geophys. Astrophys. Fluid Dyn.*, **16,** 174–206.

Orlanski, I., and E. K. M. Chang, 1993: Ageostrophic geopotential fluxes in downstream and upstream development of baroclinic waves. *J. Atmos. Sci.*, **50,** 212–225.

Papoulis, A., 1965: *Probability, Random Variables, and Stochastic Processes,* McGraw-Hill, 583 pp.

Pedlosky, J., 1987: *Geophysical Fluid Dynamics.* Springer-Verlag, 710 pp.

——, 1989: Simple models for local instabilities in zonally inhomogeneous flows. *J. Atmos. Sci.*, **46,** 1769–1778.

——, 1992: Baroclinic instability localized by dissipation. *J. Atmos. Sci.*, **49,** 1161–1170.

Petterssen, S., and S. Smebye, 1971: On the development of extratropical cyclones. *Quart. J. Roy. Meteor. Soc.*, **97,** 457–482.

Pierrehumbert, R. T., 1984: Local and global baroclinic instability in zonally inhomogeneous flows. *J. Atmos. Sci.*, **41,** 2141–2162.

Phillips, N. A., 1954: Energy transformations and meridional circulations associated with simple baroclinic waves in a two-level quasigeostrophic model. *Tellus,* **6,** 273–286.

Simmons, A. J., and B. J. Hoskins, 1978: The life cycles of some nonlinear baroclinic waves. *J. Atmos. Sci.*, **35,** 414–432.

——, and ——, 1979: The downstream and upstream development of unstable baroclinic waves. *J. Atmos. Sci.*, **36,** 1239–1254.

Stone, P. H., 1969: The meridional structure of baroclinic waves. *J. Atmos. Sci.*, **26,** 376–389.